

# Self-supervised Learning for Video Correspondence Flow

Zihang Lai

zihang.lai@cs.ox.ac.uk

Weidi Xie

weidi@robots.ox.ac.uk

Department of Computer Science  
University of Oxford, UK

Visual Geometry Group,  
Department of Engineering Science  
University of Oxford, UK

## Abstract

The objective of this paper is self-supervised learning of feature embeddings from videos, suitable for correspondence flow, *i.e.* matching correspondences between frames over the video. We leverage the natural spatial-temporal coherence of appearance in videos, to create a “pointer” model that learns to reconstruct a target frame by copying colors from a reference frame.

We make three contributions: *First*, we introduce a simple information bottleneck that enforces the model to learn robust features for correspondence matching, and avoids it learning trivial solutions, *e.g.* matching based on low-level color information. *Second*, we propose to train the model over a long temporal window in videos. To make the model more robust to complex object deformation, occlusion, *i.e.* the problem of tracker drifting, we formulate a recursive model, trained with scheduled sampling and cycle consistency. *Third*, we evaluate the approach by first training on the Kinetics dataset using self-supervised learning, and then directly applied for DAVIS video segmentation and JHMDB keypoint tracking. On both tasks, our approach has achieved state-of-the-art performance, especially on segmentation, we outperform all previous methods by a significant margin. The source code will be released at <https://github.com/zlai0/CorrFlow>.

## 1 Introduction

Correspondence matching has been the fundamental block for numerous applications ranging from depth estimation [23] to optical flow [4, 8, 12], to segmentation and tracking [36]. However, training models for correspondence matching is not a trivial task, as obtaining manual annotations can be prohibitively expensive, and sometimes are not even possible due to occlusions and objects deformations. In the recent works [32, 35], Rocco *et al.* proposed to train Convolutional Neural Networks (CNNs) for correspondence matching, where the model is first trained with artificial transformations between two input images, and further bootstrapped by training on a small dataset with human annotations. On the other hand, videos are very appealing as a data source for self-supervised learning: there is almost an infinite supply available (from YouTube etc); and there are plenty of additional proxy losses that can be employed from the intrinsic spatio-temporal coherence, *i.e.* the signals in video

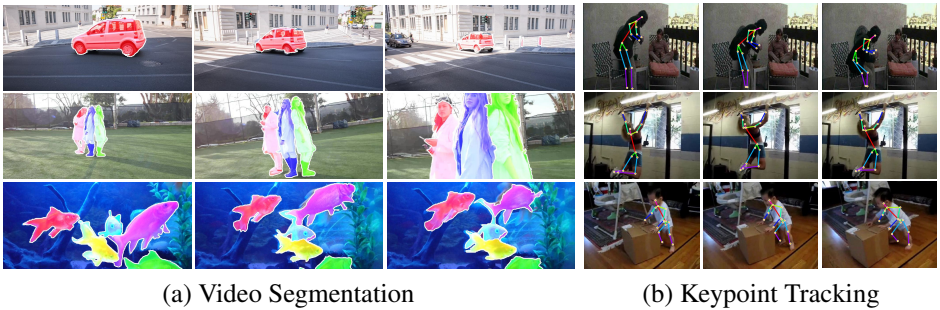


Figure 1: We propose self-supervised learning of correspondence flow on videos. Without any fine-tuning, the acquired representation generalizes to various tasks: (a) video segmentation; (b) keypoint tracking. **Note:** For both tasks, the annotation for the first frame is given, the goal is to propagate the annotations.

tend to vary smoothly in time [48, 47]. In this paper, we propose to tackle the task of dense tracking, *i.e.* correspondence flow in videos, with self-supervised learning.

We are certainly not the first one to explore this idea, in the seminal paper by Vondrick *et al.* [58], they propose to use *colorization* as a proxy task for learning video embeddings that enable correspondence matchings. During training, a pair of images are fed to a siamese feature encoder, and an affinity matrix is computed for copying colors from the reference frame. To supervise the training, a pixel-wise loss is applied between the reconstructed and ground truth target frame. In another recent work by Wang *et al.* [40], the authors propose to use cycle-consistency as the supervision signal, and train an embedding for tracking patches along with the video clip. However, as the training is based on patches, pixel-wise embedding is not necessarily optimized.

Our paper is of direct relevance to Vondrick *et al.* [58], in their work, converting RGB to grayscale image aims to set an information bottleneck for the model, which has shown to be effective in avoiding trivial solutions, *e.g.* matching by using low-level colors. However, the model trained in this way has also introduced a train-test inconsistency while deploying to the downstream task, as the model has never been trained to encode the correlation of RGB color channels in images. Moreover, as the network is only trained with a pair of ground truth video frames, it incurs the problem of model drifting on video tasks which require recursive predictions. Specifically, as the prediction for later steps will rely on the prediction from previous steps, the errors will accumulate, and there is no mechanism to enforce the model to recover from previous error states. We argue that a better framework should close the gap between training and testing as much as possible, *i.e.* the model should ideally utilize images of full RGB colors and also be trained in a recursive manner.

In this paper, we propose to solve the aforementioned challenges, and train a model for accurate video correspondence flow in a self-supervised manner. We make the following contributions:

*First*, we propose a novel idea for enforcing information bottleneck while training dense correspondence matching with raw videos. To avoid trivial solutions, we intentionally add channel-wise dropout and color jittering on the input images during training time, therefore, the model is forced *not* to rely on low-level color information, and must be robust to color jittering. This simple idea bridges the gap of inconsistency between training and testing

scenario in the early works.

*Second*, to deal with the model drifting problem, we propose to train on videos with a longer temporal window; extend the model to be recursive. We also propose to train with scheduled sampling, *i.e.* later frames will not have access to the ground truth of the previous frame; instead, they are only able to copy from the previous predictions. Meanwhile, we also impose forward-backward cycle consistency during training.

*Third*, we compare with other self-supervised learning methods, and demonstrate state-of-the-art performance on DAVIS video segmentation [60]. Moreover, we notice that training the model on Kinetics is not ideal as it is human-centric video dataset, most of the classes in DAVIS are not covered in Kinetics, *e.g.* animals. Therefore, there is no way for the model to learn semantics matching for these unseen classes. As proof of concept, we probe 10 different classes in DAVIS by downloading videos from YouTube and finetuning the model on them in a self-supervised way. Note that, we only download videos by the class labels, no segmentation annotations are used while finetuning. After self-supervised finetuning, the model shows a significant improvement on video segmentation.

## 2 Related Work

**Correspondence Matching.** Recently, researchers have studied correspondence matching in deep feature space [11, 25, 30, 32, 35]. The works from Rocco *et al.* [32, 35], propose to train deep convolutional neural networks by learning the artificial transformations between a pair of images. For robust estimation, they applied a differentiable soft inlier score for evaluating the quality of alignment between spatial features and providing a loss for learning semantic correspondences. However, their work may not be ideal as the model still relies on synthetic transformations. In contrast, we address the challenge of learning correspondence matching by exploiting the temporal coherence in videos.

**Optical Flow.** Classical variational approaches model optical flow estimation as an energy minimization problem based on brightness constancy and spatial smoothness [3]. Later works integrate feature matching to initialize sparse matching, and then interpolate into dense flow maps in a pyramidal coarse-to-fine manner [8, 33, 45]. Recent works use convolutional neural networks (CNNs) to improve sparse matching by learning an effective feature embedding [2, 20]. Another line of work is more relevant to our application, *i.e.* unsupervised optical flow learning. The basic principles are based on brightness constancy and spatial smoothness [28, 43, 49]. This leads to the most popular photometric loss that measures the difference between the reference image and the warped image, for those occluded regions, a mask is implicitly estimated by checking forward-backward consistency.

**Self-supervised Learning.** Of more direct relevance to our training framework are self-supervised frameworks that use video data [10, 7, 9, 10, 15, 16, 17, 18, 19, 21, 24, 26, 29, 38, 42, 46]. In [9, 29, 42], the proxy task is defined to focus on temporal sequence ordering of the frames. Another approach is to use the temporal coherence as a proxy loss [15, 18, 40]. Other approaches use egomotion [10, 17] in order to enforce equivariance in feature space [17]. Recently [38], leveraged the natural temporal coherency of color in videos, to train a network for tracking and correspondence related tasks. Our approach builds in particular on those that use frame synthesis [7, 19, 46], though for us synthesis is a proxy task rather than the end goal.

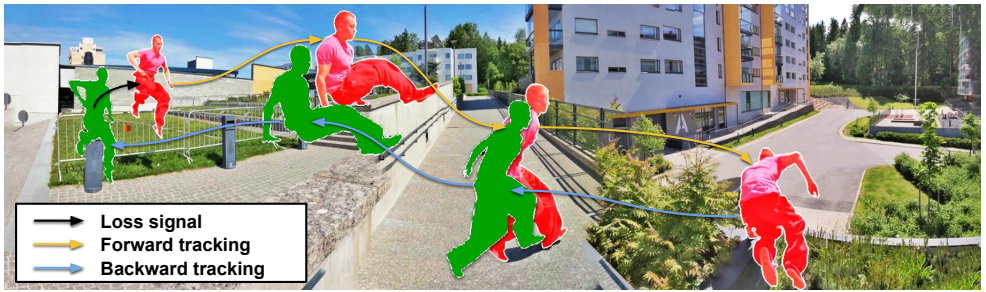


Figure 2: Self-supervised learning for correspondence flow. In our method, the dense matching is computed on feature embeddings of a longer temporal window and higher resolution; A recursive model is formulated and trained with cycle consistency.

### 3 Approach

The goal is to train an embedding network that enables dense pixelwise correspondences in a self-supervised manner, *i.e.* without any human annotations. Our basic idea is to exploit spatial-temporal coherence in videos, *i.e.* the frame appearances will not change abruptly; therefore, colors act as a reliable supervision signal for correspondence matching.

#### 3.1 Background

In this section, we briefly review the seminal work by Vondrick [38]. Let  $c_i \in \mathbb{R}^d$  be the true color for pixel  $i$  in the reference frame, and let  $c_j \in \mathbb{R}^d$  be the true color for a pixel  $j$  in the target frame.  $y_j \in \mathbb{R}^d$  is the model’s prediction for  $c_j$ , it is a linear combination of colors in the reference frame:

$$y_j = \sum_i A_{ij} c_i, \quad \text{where } A_{ij} = \frac{\exp\langle f_i^T f_j \rangle}{\sum_k \exp\langle f_k^T f_j \rangle} \quad (1)$$

$A$  is an affinity matrix computed from a simple dot product between the feature embeddings of the *grayscale* target and reference frame ( $f$ ’s). As the affinity matrix is computed from all pair of pixels, we refer to this matching process as *full attention* in the rest of this paper. As this matrix is potentially large, the authors therefore decide to compute the matching with lower resolution video frames (as shown in Figure 2 (a)).

In the following sections, we describe our novel architecture which enables to train dense correspondence tracking over long video sequences at full-color and high-resolution.

#### 3.2 Feature Embedding with Information Bottleneck

Given a collection of frames  $\{I_1, I_2, \dots, I_N\}$  from a video clip, we parametrize the feature embedding module with CNNs:

$$f_i = \Phi(g(I_i); \theta) \quad (2)$$

where  $\Phi$  refers to a feature encoder (details in Appendix), and  $g(\cdot)$  refers to the random input jittering. In our training, we randomly zero out 0, 1, or 2 channels on each input frame, each

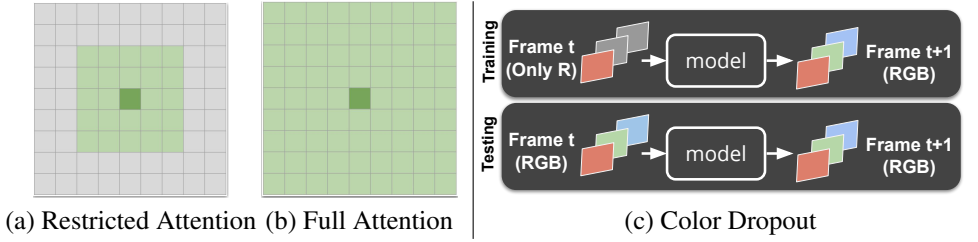


Figure 3: Restricted attention and color dropout. See text for details.

with some probability (one possible input is shown in Figure 3 (c)). We also perturb the brightness, contrast and saturation of an image by up to 10%.

Despite the simplicity, the input jittering is essentially acting as an *information bottleneck*, which avoids the model learning trivial solution for correspondence matching, and forces to instead learn high-level information for matching. While deploying for downstream tasks, images of full RGB colors are taken as input, which effectively bridges the train-test inconsistency and prevents the network from overfitting.

### 3.3 Restricted Attention

Traditionally, *full attention* has been used for computing the affinity matrix (Section 3.1), *i.e.* all pairs of pixels in target and reference frames are computed for similarity (Figure 3 (b)). However, the memory and computational consumption grow quadratically with the spatial footprint of the feature maps, thus limiting the resolution of the previous methods [68].

In fact, videos are full of regularities, *i.e.* the appearances in the video clip tend to change smoothly both spatially and temporally. To fully exploit this property, we propose to use a restricted attention mechanism (Figure 3 (a)), which leverages the spatial coherence between frames, and leading to both an increase of feature resolution for correspondence matching, as well as a decrease in memory and computation consumption. Specifically, we impose a maximum disparity of  $M$  - that is, pixels in the reference frame  $t$  is searched locally in a square patch of size  $(2M+1) \times (2M+1)$ , centered at the target pixel. Suppose the feature maps have a dimension of  $H \times W$ , the affinity volume ( $A$ ) is therefore a 4D tensor of dimension  $H \times W \times (2M+1) \times (2M+1)$ . The  $(i, j, k, l)$  entry of the tensor denotes the similarity between pixel  $(i, j)$  of the target frame, and pixel  $(i+k-M, j+l-M)$  of the reference frame.

$$A^{ijkl} = \frac{\exp \langle f_t^{(i+k-M)(j+l-M)}, f_{t+1}^{ij} \rangle}{\sum_p \sum_q \exp \langle f_t^{(i+q)(j+p)}, f_{t+1}^{ij} \rangle} \quad (3)$$

$$\hat{I}_{t+1} = \psi(A_{(t,t+1)}, I_t) = \sum_p \sum_q A^{ij(p+M)(q+M)} I_t \quad (4)$$

where  $f_t = \Phi(g(I_t); \theta)$  and  $f_{t+1} = \Phi(g(I_{t+1}); \theta)$ , referring to the feature embedding for frame  $t$  and  $t+1$  respectively,  $\psi()$  refers to the soft-copy operation, and  $p, q \in [-M, M]$  and  $\hat{I}_{t+1}$  refers to the reconstruction of  $t+1$  frame by copying colors from  $I_t$  frame.

### 3.4 Long-term Correspondence Flow

One of the major challenges on self-supervised learning of correspondence flow is how to sample the frames for training; if two frames are sampled very closely in the temporal axis, the objects will not change dramatically either in appearance or spatial position, the matching becomes an easy task and the model will not benefit from training on them. Empirically, in self-supervised learning, more difficult tasks usually lead to better representations [26]. Clearly, the natural way to increase the task difficulty is to sample frames with a large temporal stride in the video. However, under this situation, our fundamental assumption about using reconstruction as supervision may fail, due to object deformation, illumination change, motion blurs, and occlusions.

In this section, we propose two approaches to improve the model’s robustness to drifting, and gently bridge the gap of training with either too easy or too hard samples, *i.e.* scheduled sampling, and cycle consistency.

#### 3.4.1 Scheduled Sampling

Scheduled sampling is a widely used curriculum learning strategy for sequence-to-sequence models [9], the main idea is to replace some ground truth tokens by the model’s prediction, to improve the model robustness to wrong predictions, and bridge the gap between how the model is used at training and inference.

In our case, for  $n$  frames in a video sequence, a shared embedding network is used to get feature embeddings ( $f_i = \Phi(g(I_i); \theta)$  where  $i = 1, \dots, n$ ), the reconstruction is therefore formalized as a recursive process:

$$\hat{I}_n = \begin{cases} \psi(A_{(n-1,n)}, I_{n-1}) & (1) \\ \psi(A_{(n-1,n)}, \hat{I}_{n-1}) & (2) \end{cases}$$

while reconstructing the  $n$ th frame ( $\hat{I}_n$ ), the model may have access to the previous frame as either groundtruth ( $I_{n-1}$ ) or model prediction ( $\hat{I}_{n-1}$ ). During training, the probability of using ground truth frames starts from a higher value (0.9) in early training stage (case (1)), and is then uniformly annealed to a probability of 0.6 (case (2)). Note that, as the model has been formulated to be recursive, the idea of scheduled sampling has effectively handled the drifting problem, as the model is forced to be robust and recover from the error states.

#### 3.4.2 Cycle Consistency

Following the scheduled sampling, we also explicitly adopt cycle consistency for training correspondence flow. Unlike the recent work [21], we do not use the cycle consistency as the dominating supervision signal; instead, it is treated as another regularizer for combating tracker drifting. During training, we apply our tracker  $n$  frames forward and backward to the current frame, which is required to be the same as the true current frame.

### 3.5 Learning Objectives

Similar to the previous work [33], we pose frame reconstruction as a classification problem. In our implementation, the color is quantized into 16 classes with K-means clustering on the



*Lab* space of frames. The objective function is defined as :

$$L = \alpha_1 \cdot \sum_{i=1}^n \mathcal{L}_1(I_i, \hat{I}_i) + \alpha_2 \cdot \sum_{j=n}^1 \mathcal{L}_2(I_j, \hat{I}_j) \quad (5)$$

where  $\mathcal{L}_1, \mathcal{L}_2$  refers to the pixel-wise cross entropy between groundtruth and reconstructed frames in the *forward* and *backward* pass respectively, the loss weights are  $\alpha_1 = 1, \alpha_2 = 0.1$ .

## 4 Experiments and Analysis

In the following sections, we start with the training details, and provide ablation studies to show the effectiveness of proposed components on the video segmentation task, *e.g.* color dropout, cycle consistency, scheduled sampling, restricted attention.

**Training Details** In this paper, we train CNNs in a completely unsupervised fashion, meaning we do not use any information other than video sequences, and we do not finetune for a target task. In all of our experiments, we use a variant of ResNet-18 as a feature encoder (the architecture details can be found in Appendix), the CNNs end up with feature embeddings  $1/4$  of the original image size, we set the max disparity  $M$  as 6 (as described in Section 3.3). The temporal length  $n$  is set to 3 in our case, when considering the forward-backward cycles, the effective sequence length is actually 6 (forward-backward). We train our model end-to-end using a batch size of 8 for 1M iterations with an Adam optimizer. The initial learning rate is set to  $2e^{-4}$ , and is halved on 0.4, 0.6 and 0.8M iterations. The model is trained on Kinetics [22] without using any class label. As pre-processing, we decode the videos with a frame rate of 6fps, and resize all frames to  $256 \times 256 \times 3$ .

**Evaluation Metrics** In this paper, we report results on two public benchmarks: video segmentation, and pose keypoint propagation. For both tasks, a ground truth annotation is given for the first frame, and the objective is therefore to propagate the mask to later frames. In video segmentation, we test our model on DAVIS-2017 [82], and evaluate on two standard metrics, region overlapping ( $\mathcal{J}$ ) and contour accuracy ( $\mathcal{F}$ ). For pose keypoint tracking, we evaluate our model on JHMDB dataset. We use two different PCK metrics. The first ( $\text{PCK}_{instance}$ ) considers a keypoint correct if the Normalized Euclidean Distance between that keypoint and the ground truth is smaller than a threshold  $\alpha$ . The second ( $\text{PCK}_{max}$ ) accepts a keypoint if it is located within  $\alpha \cdot \max(w, h)$  pixels of the ground truth, where  $w$  and  $h$  are the width and height of the instance bounding box.

### 4.1 Video Segmentation on DAVIS-2017

#### 4.1.1 Ablation Studies

To examine the effects of different components, we conduct a series of ablation studies. All models are trained from scratch on Kinetics, and evaluated on the video segmentation task (DAVIS-2017) without finetuning as shown in Table 1. More detailed analysis can be found in the Appendix.

**Color Dropout** Instead of taking full-color input, frames are converted to grayscale and passed in as inputs, same as Vondrick *et al.* [68]. As shown in the Table 1, the error increased

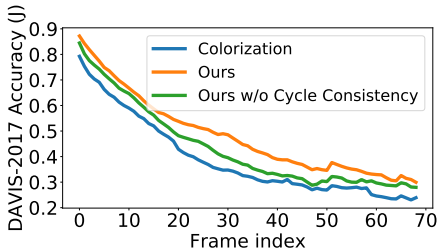


Figure 4: Ablation studies on drifting. The proposed model with cycle consistency has shown to be most robust as masks propagate.

| Method                        | $\mathcal{J}(\text{Mean})$ | $\mathcal{F}(\text{Mean})$ |
|-------------------------------|----------------------------|----------------------------|
| Ours (Full Model)             | 47.7                       | 51.3                       |
| Ours w/o Color Dropout        | 40.5                       | 39.5                       |
| Ours w/o Restricted Attention | 40.8                       | 39.7                       |
| Ours w/o Cycle Consistency    | 41.0                       | 40.4                       |
| Ours w/o Scheduled Sampling   | 40.2                       | 39.2                       |

Table 1: Ablation Studies on DAVIS-2017.  $\mathcal{J}$ : region overlapping,  $\mathcal{F}$ : contour accuracy respectively.

significantly by 7.2% in  $\mathcal{J}$  and 11.8% in  $\mathcal{F}$ . This demonstrates the importance of bridging the discrepancy between training and testing on color information.

**Restricted Attention** We modify the similarity matching procedure by removing the restricted attention module. Specifically, the full attention model makes use of over 9.2G of GPU memory to process a single 480p image, making it impossible to train on HD images with large batch size. In comparison, our original model with restricted attention only takes 1.4G GPU memory for the same image. As table 1 shows, performance dropped by 6.9% and 11.6% respectively. This decrease confirms that we need to uphold spatial coherence between video frames: while it is possible that multiple similar objects co-exist in a frame, distant objects are unlikely to match up because of the coherence requirement. By utilizing this prior knowledge, our restricted attention could lead to better correspondences.

**Scheduled Sampling** When disabling the scheduled sampling during training, *i.e.* all frames used for copying are ground truth, the performance dropped significantly, suggesting the effectiveness of scheduled sampling on bridging the train-test gap, where ground truth from the previous frame is not available.

**Cycle Consistency** Lastly, we evaluate the forward-backward consistency for solving the drifting problem. As seen in Figure 4, while both models start off with high accuracy early in a video sequence, the model with cycle-consistency performs better in later stages of video sequences, indicating a less severe drifting problem. This can also be reflected in the quantitative analysis, where cycle consistency enables a performance boost by 7.5% in mIoU and 12.1% in boundary accuracy.

#### 4.1.2 Comparison with State-of-the-art

In Table 2, we show the results of our full model on the DAVIS-2017 benchmark. Our model clearly dominates all the unsupervised method, while also approaching the results of some supervised methods. In Figure 6, we provide the qualitative prediction from our correspondence flow model (more results in Appendix). The segmentation mask can be propagated through sequences even when facing significant scale variation from camera motion, and object deformations.



| Method                             | Supervised   | $\mathcal{J} \& \mathcal{F}$ (Mean) | $\mathcal{J}$ (Mean) | $\mathcal{J}$ (Recall) | $\mathcal{F}$ (Mean) | $\mathcal{F}$ (Recall) |
|------------------------------------|--------------|-------------------------------------|----------------------|------------------------|----------------------|------------------------|
| Identity                           | $\times$     | 22.9                                | 22.1                 | 15.9                   | 23.6                 | 11.7                   |
| Optical Flow (FlowNet2) [14]       | $\times$     | 26.0                                | 26.7                 | -                      | 25.2                 | -                      |
| SIFT Flow [2]                      | $\times$     | 34.0                                | 33.0                 | -                      | 35.0                 | -                      |
| Transitive Inv. [11]               | $\times$     | 29.4                                | 32.0                 | -                      | 26.8                 | -                      |
| DeepCluster [43]                   | $\times$     | 35.4                                | 37.5                 | -                      | 33.2                 | -                      |
| Video Colorization [33]            | $\times$     | 34.0                                | 34.6                 | 34.1                   | 32.7                 | 26.8                   |
| CycleTime (ResNet-50) [41]         | $\times$     | 40.7                                | 41.9                 | 40.9                   | 39.4                 | 33.6                   |
| <b>Ours (Full Model ResNet-18)</b> | $\times$     | <b>49.5</b>                         | <b>47.7</b>          | <b>53.2</b>            | <b>51.3</b>          | <b>56.5</b>            |
| ImageNet (ResNet-50) [14]          | $\checkmark$ | 49.7                                | 50.3                 | -                      | 49.0                 | -                      |
| SiamMask [39]                      | $\checkmark$ | 53.1                                | 51.1                 | 60.5                   | 55.0                 | 64.3                   |
| OSVOS [8]                          | $\checkmark$ | 60.3                                | 56.6                 | 63.8                   | 63.9                 | 73.8                   |

Table 2: Video segmentation results on DAVIS-2017 dataset. Higher values are better.

### 4.1.3 Probing Upper bound of Self-supervised Learning

Despite the superior performance on the video segmentation task, we notice that training models on Kinetics are not ideal, as it is a human-centric video dataset. Most of the classes in DAVIS are not covered in Kinetics, *e.g.* cars, animals; therefore, there is no way the model can learn semantics about these unseen classes.

As proof of concept, we probe 8 DAVIS classes by downloading videos from YouTube and finetuning our model on them in a self-supervised manner. Note that, we only download videos by the class labels, and no segmentation annotations are used while finetuning. We show the video segmentation results in Figure 9 (more results can be found in the Appendix). As the number of training videos increases, all sequences have shown performance boosts on both metrics ( $\mathcal{J}, \mathcal{F}$ ).

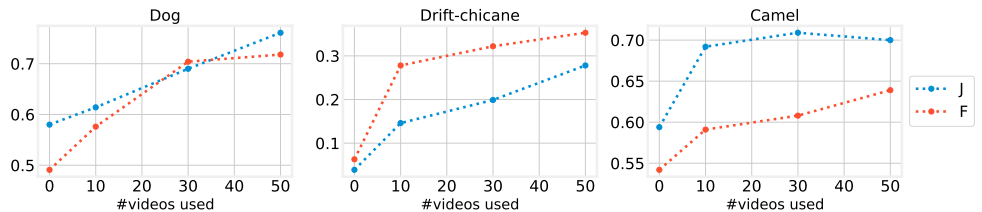


Figure 5: Results after self-supervised finetuning on more YouTube videos.

## 4.2 Keypoint Tracking on JHMDB

As shown in Table 3, our approach exceeds the previous methods [33] by an average of 11.3% in  $\text{PCK}_{instance}$ . Also, we achieve a higher gain in the more strict  $\text{PCK}@.1$  metric when compared to the recent patch-based CycleTime [41]. This suggests that a more precise pixel-level embedding is learned. Interestingly, our method even outperforms the state-of-the-art supervised method [67] in  $\text{PCK}_{max}$ .

| Method                             | Supervised | PCK <sub>instance</sub> |             | PCK <sub>max</sub> |             |
|------------------------------------|------------|-------------------------|-------------|--------------------|-------------|
|                                    |            | @.1                     | @.2         | @.1                | @.2         |
| SIFT Flow [12]                     | ✗          | 49.0                    | 68.6        | -                  | -           |
| Video Colorization [13]            | ✗          | 45.2                    | 69.6        | -                  | -           |
| CycleTime (ResNet-50) [14]         | ✗          | 57.7                    | 78.5        | -                  | -           |
| <b>Ours (Full Model ResNet-18)</b> | ✗          | <b>58.5</b>             | <b>78.8</b> | <b>71.9</b>        | <b>88.3</b> |
| ImageNet (ResNet-50) [15]          | ✓          | 58.4                    | 78.4        | -                  | -           |
| Fully Supervised [8]               | ✓          | -                       | -           | 68.7               | 81.6        |

Table 3: Keypoint tracking on JHMDB dataset (Validation split 1). Higher values are better.

## 5 Conclusion

We presented an algorithm for pixel-level correspondence matching learned from raw videos in a self-supervised fashion. We propose a novel information bottleneck that enables the model to be trained on standard RGB images, and close the gap between training and testing. To alleviate the problem from model drifting, we formulate the model in a recursive manner, trained with scheduled sampling and cycle consistency. We demonstrated state-of-the-art performance on two different tasks with our model simply trained on the human-focused Kinetics dataset. Moreover, we also probe the upper bound of our self-supervised learning by finetuning on larger and more diverse video datasets. We believe self-supervised learning for correspondence flow is far from saturation. All code and pre-trained model available open source upon acceptance.

## Acknowledgment

We thank Erika Lu, Tengda Han for the insightful discussions. Financial support was provided by EPSRC Seebibyte Grant EP/M013774/1.

## References

- [1] P. Agrawal, J. Carreira, and J. Malik. Learning to see by moving. In *Proc. ICCV*, 2015.
- [2] C. Bailer, K. Varanasi, and D. Stricker. Cnn-based patch matching for optical flow with thresholded hinge embedding loss. In *Proc. CVPR*, 2017.
- [3] S. Bengio, O. Vinyals, N. Jaitly, and N. Shazeer. Scheduled sampling for sequence prediction with recurrent neural networks. In *NIPS*, 2015.
- [4] T. Brox, A. Bruhn, N. Papenberger, and J. Weickert. High accuracy optical flow estimation based on a theory for warping. In *Proc. ECCV*, 2004.
- [5] T. Brox, C. Bregler, and J. Malik. Large displacement optical flow. In *Proc. CVPR*, 2009.
- [6] S. Caelles, K.K. Maninis, J. Pont-Tuset, L. Leal-Taixé, D. Cremers, and L. Van Gool. One-shot video object segmentation. In *Proc. CVPR*, 2017.

- [7] E.L. Denton and V. Birodkar. Unsupervised learning of disentangled representations from video. In *NIPS*, 2017.
- [8] A. Dosovitskiy, P. Fischer, E. Ilg, P. Hausser, C. Hazirbas, V. Golkov, P. Smagt, D. Cremers, and T. Brox. FlowNet: Learning optical flow with convolutional networks. In *Proc. ICCV*, 2015.
- [9] B. Fernando, H. Bilen, E. Gavves, and S. Gould. Self-supervised video representation learning with odd-one-out networks. In *CVPR*, 2017.
- [10] C. Gan, B. Gong, K. Liu, H. Su, and L. J. Guibas. Geometry guided convolutional neural networks for self-supervised video representation learning. In *Proc. CVPR*, 2018.
- [11] K. Han, R.S. Rezende, B. Ham, K.Y.K. Wong, M. Cho, C. Schmid, and J. Ponce. Scnet: Learning semantic correspondence. In *Proc. ICCV*, 2017.
- [12] K. He, X. Zhang, S. Ren, and J. Sun. Deep residual learning for image recognition. In *Proc. CVPR*, 2016.
- [13] B. K. P. Horn and B. G. Schunck. Determining optical flow. *Artificial Intelligence*, 17: 185–203, 1981.
- [14] E. Ilg, N. Mayer, T. Saikia, M. Keuper, A. Dosovitskiy, and T. Brox. FlowNet 2.0: Evolution of optical flow estimation with deep networks. In *Proc. CVPR*, 2017.
- [15] P. Isola, D. Zoran, D. Krishnan, and E.H. Adelson. Learning visual groups from co-occurrences in space and time. In *Proc. ICLR*, 2015.
- [16] T. Jakab, A. Gupta, H. Bilen, and A. Vedaldi. Conditional image generation for learning the structure of visual objects. In *NIPS*, 2018.
- [17] D. Jayaraman and K. Grauman. Learning image representations tied to ego-motion. In *Proc. ICCV*, 2015.
- [18] D. Jayaraman and K. Grauman. Slow and steady feature analysis: higher order temporal coherence in video. In *Proc. CVPR*, 2016.
- [19] X. Jia, B. De Brabandere, and T. Tuytelaars. Dynamic filter networks. In *NIPS*, 2016.
- [20] X. Jia, R. Ranftl, and V. Koltun. Accurate optical flow via direct cost volume processing. In *Proc. CVPR*, 2017.
- [21] L. Jing and Y. Tian. Self-supervised spatiotemporal feature learning by video geometric transformations. *arXiv preprint arXiv:1811.11387*, 2018.
- [22] W. Kay, J. Carreira, K. Simonyan, B. Zhang, C. Hillier, S. Vijayanarasimhan, Viola F., T. Green, P. Natsev, M. Suleyman, and A. Zisserman. The kinetics human action video dataset. 2017.
- [23] A. Kendall, H. Martirosyan, S. Dasgupta, P. Henry, R. Kennedy, A. Bachrach, and A. Bry. End-to-end learning of geometry and context for deep stereo regression. In *Proc. CVPR*, 2017.

- [24] D. Kim, D. Cho, and I. S. Kweon. Self-supervised video representation learning with space-time cubic puzzles. In *AAAI*, 2018.
- [25] S. Kim, D. Min, B. Ham, S. Jeon, S. Lin, and K. Sohn. Fcss: Fully convolutional self-similarity for dense semantic correspondence. In *Proc. CVPR*, 2017.
- [26] H.Y. Lee, J.B. Huang, M. Singh, and M.H. Yang. Unsupervised representation learning by sorting sequences. In *Proc. ICCV*, 2017.
- [27] C. Liu, J. Yuen, and A. Torralba. Sift flow: Dense correspondence across scenes and its applications. *IEEE transactions on pattern analysis and machine intelligence*, 2011.
- [28] S. Meister, J. Hur, and S. Roth. UnFlow: Unsupervised learning of optical flow with a bidirectional census loss. In *AAAI*, 2018.
- [29] I. Misra, C. L. Zitnick, and M. Hebert. Shuffle and learn: Unsupervised learning using temporal order verification. In *ECCV*, 2016.
- [30] D. Novotny, D. Larlus, and A. Vedaldi. AnchorNet: A weakly supervised network to learn geometry-sensitive features for semantic matching. In *Proc. CVPR*, 2017.
- [31] F. Perazzi, J. Pont-Tuset, B. McWilliams, L. Van Gool, M. Gross, and A. Sorkine-Hornung. A benchmark dataset and evaluation methodology for video object segmentation. In *Proc. CVPR*, 2016.
- [32] J. Pont-Tuset, Perazzi. F., S. Caelles, P. Arbeláez, A. Sorkine-Hornung, and L. Van Gool. The 2017 davis challenge on video object segmentation. *arXiv:1704.00675*, 2017.
- [33] J. Revaud, P. Weinzaepfel, Z. Harchaoui, and C. Schmid. Epicflow: Edge-preserving interpolation of correspondences for optical flow. In *Proc. CVPR*, 2015.
- [34] I. Rocco, R. Arandjelovic, and J. Sivic. Convolutional neural network architecture for geometric matching. In *Proc. CVPR*, 2017.
- [35] I. Rocco, R. Arandjelovic, and J. Sivic. End-to-end weakly-supervised semantic alignment. In *Proc. CVPR*, 2018.
- [36] S.M. Smith and J.M. Brady. Asset-2: Real-time motion segmentation and shape tracking. *IEEE Transactions on Pattern Analysis and Machine Intelligence*, 17(8):814–820, 1995.
- [37] J. Song, L. Wang, L. Van Gool, and O. Hilliges. Thin-slicing network: A deep structured model for pose estimation in videos. In *Proc. CVPR*, 2017.
- [38] C. Vondrick, A. Shrivastava, A. Fathi, S. Guadarrama, and K. Murphy. Tracking emerges by coloring videos. In *Proc. ECCV*, 2018.
- [39] Q. Wang, L. Zhang, L. Bertinetto, W. Hu, and P.H.S Torr. Fast online object tracking and segmentation: A unifying approach. In *Proc. CVPR*, 2019.
- [40] X. Wang, K. He, and A. Gupta. Transitive invariance for self-supervised visual representation learning. In *Proc. CVPR*, 2017.

- [41] X. Wang, A. Jabri, and A. Efros. Learning correspondence from the cycle-consistency of time. In *Proc. CVPR*, 2019.
- [42] X.L Wang and A. Gupta. Unsupervised learning of visual representations using videos. In *ICCV*, 2015.
- [43] Y. Wang, Y. Yang, Z. Yang, L. Zhao, P. Wang, and W. Xu. Occlusion aware unsupervised learning of optical flow. In *Proc. CVPR*, 2018.
- [44] D.L. Wei, J.J. Lim, A. Zisserman, and W.T. Freeman. Learning and using the arrow of time. In *CVPR*, 2018.
- [45] P. Weinzaepfel, J. Revaud, Z. Harchaoui, and C. Schmid. DeepFlow: Large displacement optical flow with deep matching. In *Proc. ICCV*, pages 1385–1392, 2013.
- [46] O. Wiles, A.S. Koepke, and A. Zisserman. X2face: A network for controlling face generation using images, audio, and pose codes. In *Proc. ECCV*, 2018.
- [47] L. Wiskott and T. Sejnowski. Slow feature analysis: Unsupervised learning of invariances. In *Neural Computation*, 2002.
- [48] J. Xie, R. Girshick, and A. Farhadi. Unsupervised deep embedding for clustering analysis. In *Proc. ICML*, 2016.
- [49] J.J. Yu, A.W. Harley, and K.G. Derpanis. Back to basics: Unsupervised learning of optical flow via brightness constancy and motion smoothness. In *Proc. ECCV*, 2016.

## Appendix A Network architecture

We use a modified ResNet-18[17] architecture with enlarged output feature maps size. Details of the network can be found below.

| 0                 | Input image   |
|-------------------|---|
| Feature extractor |   |
| 1                 | $7 \times 7$ conv with stride 2 and 64 filters            |
| 2                 | $3 \times 3$ Residual Block with stride 1 and 64 filters  |
| 3                 | $3 \times 3$ Residual Block with stride 2 and 128 filters |
| 4                 | $3 \times 3$ Residual Block with stride 1 and 256 filters |
| 5                 | $3 \times 3$ Residual Block with stride 1 and 256 filters |

Table 4: Network architecture. A Residual Block stands for a residually connected sequence of operations: convolution, batch normalization, rectified linear units (ReLU), convolution, batch normalization. See [17] for details.

## Appendix B Additionnal results on DAVIS-2017

### B.1 Qualitative results

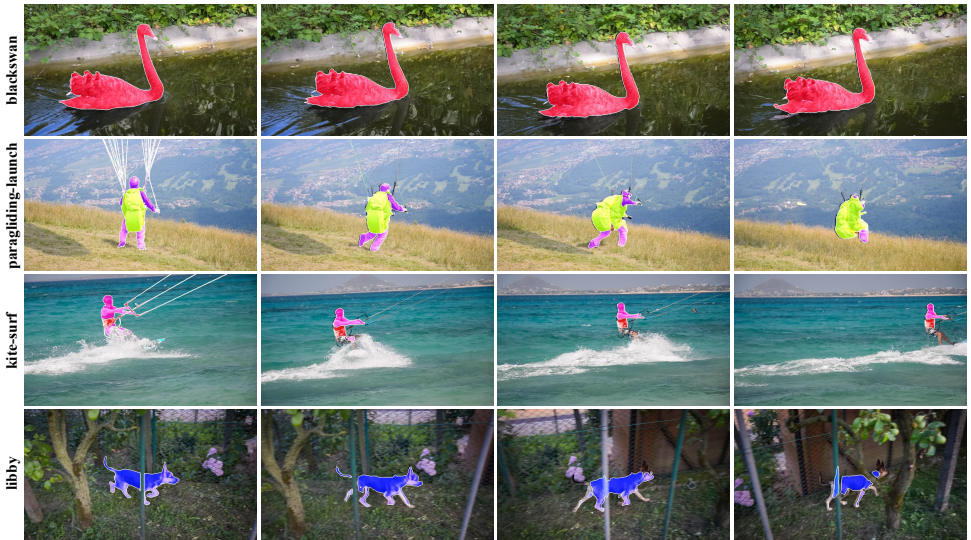


Figure 6: Additional qualitative results on DAVIS-2017.

In Figure 6, we show more predictions results from our model trained on Kinetics, and directly used for mask propagation on DAVIS, *i.e.* no finetuning has been done. Note that, the 2nd, 3rd, and 4th row shows very challenging scenarios, where the objects are under deformation, or slightly occluded. Yet, our model still performs favorably well.

### B.2 Accuracy by attributes

In Figure 7, we show DAVIS-2017 testing accuracy grouped into different categories. The proposed method has shown to outperform the previous methods in all situations. Specifi-



cally, on the color-related classes, *e.g.* Background Clutter, Interactive Objects, our method has gained significant performance boost, suggesting that our model learned better feature embeddings by using full-color inputs.

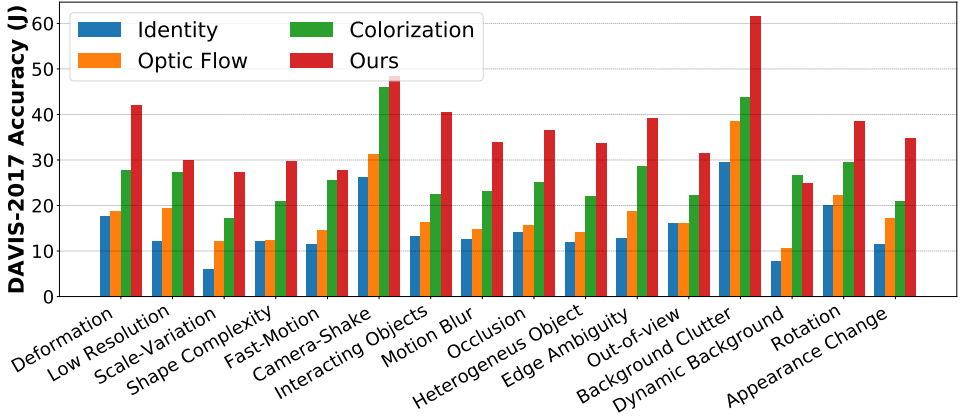


Figure 7: Accuracy by attributes.

### B.3 Failure cases

Figure 8 demonstrates some failure cases during mask propagation. Row 1 shows our tracker fails due to occlusions. As we only use the mask of the previous frame to propagate, an object is unlikely to be retrieved after it’s occluded. Similarly, it is difficult to recover an object once it goes out of the frame (Row 2). Lastly, if the object is under complex deformation, it is likely to incur the model drifting from ideal predictions.

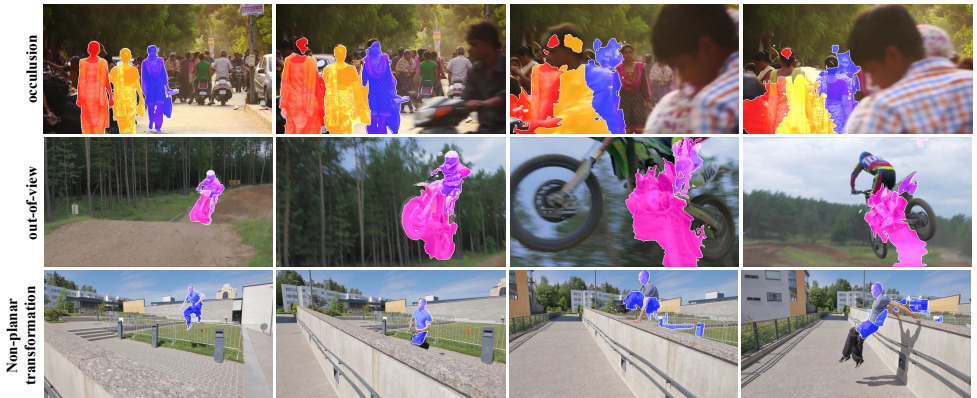


Figure 8: Common failed cases, including occlusion, out-of-view and complex transformation.

## Appendix C Additional results of fine-tuning

### C.1 Qualitative results of fine-tuning

In this part, we show the results from finetuning on videos from 8 probed classes from DAVIS-2017. Note that, we only download videos by the class labels, and no segmentation annotations are used while finetuning. As the number of training videos increases, all sequences have shown performance boosts on both metrics ( $\mathcal{J}$ ,  $\mathcal{F}$ ). Some classes (*e.g.* Dog) show a large performance gain from finetuning, as the model’s performance increases up until a complete set of 50 videos is given. Some classes (*e.g.* Camel) plateaued soon after fine-tuning on 10-30 videos. We conjecture this is due to the fact that the former set of classes contain high variance in shapes, whereas the latter set of classes have relatively more rigid shapes.

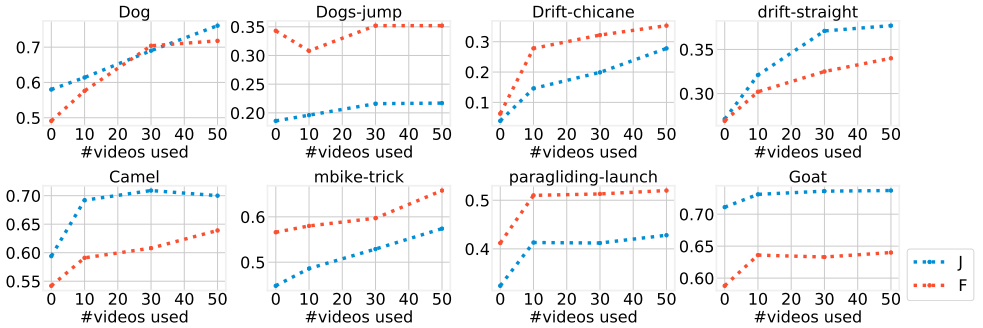


Figure 9: Fine-tuning results for additional classes.

### Numerical results

| Method                              | Dog  | Dog-j | Drift-c | Drift-s | Camel | Mbike | Paragliding | Goat |
|-------------------------------------|------|-------|---------|---------|-------|-------|-------------|------|
| No fine-tuning ( $\mathcal{J}$ )    | 58.0 | 18.6  | 3.9     | 27.1    | 59.4  | 44.8  | 32.4        | 71.1 |
| After fine-tuning ( $\mathcal{J}$ ) | 76.1 | 21.7  | 27.8    | 37.7    | 70.0  | 57.4  | 42.8        | 73.7 |
| Supervised ( $\mathcal{J}$ )        | 87.7 | 38.8  | 4.9     | 66.4    | 88.4  | 72.5  | 38.0        | 80.4 |
| No fine-tuning ( $\mathcal{F}$ )    | 49.1 | 34.3  | 6.3     | 26.9    | 54.2  | 56.6  | 41.2        | 58.8 |
| After fine-tuning ( $\mathcal{F}$ ) | 71.8 | 35.2  | 35.3    | 34.0    | 63.9  | 65.8  | 52.0        | 64.0 |
| Supervised ( $\mathcal{F}$ )        | 84.6 | 45.2  | 8.4     | 57.7    | 92.2  | 76.7  | 58.1        | 74.7 |